Journal of the Serbian Chemical Society
JSCS@tmf.bg.ac.rs • www.shd.org.rs/JSCS
J. Serb. Chem. Soc. *89* (11) 1475–1487 (2024)
JSCS–5801
Original scientific paper
Published 3 December, 2024

Thermal behavior of polymeric nickel(II) oxalate complex obtained through nickel(II) nitrate/ethylene glycol reaction

MIRCEA NICULESCU[1], MIHAI-COSMIN PASCARIU[2,3]*, ANDREI RACU[2] and BOGDAN-OVIDIU TARANU[2]**

[1]University Politehnica Timisoara, Faculty of Industrial Chemistry and Environmental Engineering, 6 Vasile Parvan Blvd., RO-300223 Timisoara, Romania, [2] National Institute of Research and Development for Electrochemistry and Condensed Matter, 144 Dr. Aurel Paunescu-Podeanu, RO-300569 Timisoara, Romania and [3]"Vasile Goldis" Western University of Arad, Faculty of Pharmacy, 86 Liviu Rebreanu, RO-310414 Arad, Romania

(Received 13 October, revised 25 December 2023, accepted 18 August 2024)

Abstract: This paper describes the analysis of the thermal decomposition of polymeric nickel (II) oxalate complex, a homopolynuclear coordination compound having the formula $[Ni(C_2O_4)(H_2O)_2]_n \cdot xnH_2O$. The thermolysis was conducted in both dynamic oxidative and inert atmospheres by simultaneously applying thermogravimetry (TG), differential thermogravimetry (DTG) and differential thermal analysis (DTA). The proposed decomposition mechanism was confirmed using evolved gas analysis (EGA) technique *via* the Fourier transform infrared spectroscopy (FTIR) of the gaseous decomposition products. The solid-state decomposition products formed during heating were investigated by chemical analysis, FTIR, Raman spectroscopy and X-ray diffraction (XRD). The structure, morphology and properties of the final decomposition products were characterized by XRD, FTIR, energy dispersive X-ray spectroscopy (EDX) and transmission electron microscopy (TEM). These analyses show that the final decomposition product in oxidative atmosphere was nickel oxide, shaped as polygonal particles with widely distributed sizes. As for the results in inert atmosphere, they outlined a mixture of Ni and NiO as rhombohedral particles in a 3:2 mole ratio.

Keywords: homopolynuclear coordination compound; nickel oxide; evolved gas analysis.

INTRODUCTION

Oxide systems, generated through various methods, are nowadays required in increasing quantities because of the development of modern technologies in many

* Corresponding authors. E-mail: (*)mihai.cosmin.pascariu@gmail.com, (**)b.taranu84@gmail.com
https://doi.org/10.2298/JSC231013071N

fields such as sensing, environmental remediation, energy storage and conversion, catalysis, optoelectronics, photonics and pharmaceuticals.[1] One of the synthetic pathways used for their preparation consists in the thermal conversion of homo- and heteropolynuclear metal complexes, which contain anions of carboxylic acids as ligands.[2]

Previous papers[2–4] have described the products of the redox reactions between several diols, such as ethylene glycol, 1,2-propanediol and 1,3-propanediol and certain metal nitrates. All the coordination compounds obtained through this method contain carboxylate or hydroxycarboxylate anions as ligands (*i.e.*, glyoxylate, oxalate, lactate or 3-hydroxypropionate). These complexes, which contain simple organic ligands, have one main advantage over other coordination compounds: they undergo thermally induced degradation to metals, alloys and oxide structures at considerably low temperatures, with the release of gaseous species such as carbon oxides (CO, CO_2), hydrocarbons (*e.g.*, CH_4) and water. The composition of the obtained powders depends on both the structure of the coordination compound and the thermal treatment being applied.

A variety of preparative methods allow for the production of nickel oxides with specific properties regarding their crystallinity degree, particle size (from nm to mm), morphology and surface area.[5]

Nanosized materials have attracted many researchers because of their unusual properties based on the size-quantization effect and the large surface area. Nanosized nickel oxide is of great interest because it exhibits anomalous electronic[6] and magnetic[7] properties. The characteristic properties of nanosized NiO particles also enable one to tailor materials for various applications, including catalysis,[8] electrochromic windows[9] and sensors.[10] These properties can be enhanced by decreasing the particle size, on which they are highly dependent. This is why precise control of the size and distribution in the nanometre regime is required. In addition, a facile preparation process that allows the convenient production of these particles is necessary for miscellaneous new applications. So far, many different methods have been attempted to synthesize nanosized NiO, such as thermal decomposition,[11,12] microemulsion,[13] precipitation,[14,15] electrochemical deposition,[16] sol–gel technique[17,18] and surfactant-mediated method.[19]

The present paper aims to clarify the mechanism involved in the thermal decomposition of polymeric nickel(II) oxalate complex, namely nickel(II) oxalate dihydrate having the formula $[Ni(C_2O_4)(H_2O)_2]_n \cdot xnH_2O$,[20] in both oxidative and inert atmospheres. Macklen[21] analysed the thermal behaviour of the simple nickel (II) oxalate dihydrate obtained through classical methods. On the other hand, our study refers to a polynuclear compound obtained by an original method, starting from nickel (II) nitrate and ethylene glycol in the presence of nitric acid. The *in situ* generation of the ligand, the oxalate anion, simultaneously with its coordination to the complex generator, Ni^{2+}, leads to a polynuclear structure, which pos-

sesses high stability: it is virtually insoluble in water and common organic solvents, and it can only be decomposed in a strongly acidic medium.[20] This study also shows that, following the thermal decomposition at relatively low temperatures of this complex compound, nickel oxide is obtained in oxidative atmosphere, while a mixture of nickel oxide and nickel is produced in inert atmosphere.

EXPERIMENTAL

$[Ni(C_2O_4)(H_2O)_2]_n \cdot xnH_2O$ was prepared starting from nickel (II) nitrate hexahydrate (Merck) and ethylene glycol (Sigma–Aldrich), in the presence of nitric acid (Sigma–Aldrich), using an original method, as described in a previous paper.[20] The compound was purified by refluxing in a 5:1 by volume acetone/water mixture (acetone from Chimreactiv Bucharest) in an ultrasonic bath before being used.

For the thermal analysis, a Netzsch STA 409 PC coupled with a Bruker 27 FTIR instrument (for evolved gas detection) was used, with the following measuring conditions: 10 °C min^{-1} heating speed, 100 mL min^{-1} synthetic air flow and 20.58 mg sample weight for the oxidative decomposition, as well as a gas flow rate of 100 mL min^{-1} and a 30.00 mg sample weight in dynamic atmosphere of argon.

The phase composition of the powders obtained through the complex's thermolysis at 400 and 1000 °C was investigated by X-ray diffractometry (XRD) using a Rigaku Ultima IV diffractometer with CuK_α radiation (λ = 1.5406 Å). The lattice parameters (*a*, *b*, *c*) and the average crystallite size (*d*) were calculated by using the whole pattern profile fitting (WPPF) method. The instrument influence over the lines' broadening was subtracted using the diffraction pattern of a Si standard recorded in the same conditions.

The FTIR spectra of the solid products were acquired on a Vertex 70 (Bruker, Germany) FT-IR spectrometer in the 4000–400 cm^{-1} domain, using KBr pellets.

The Raman spectra were measured at room temperature using a MultiView-1000 system (Nanonics Imaging, Israel) incorporating the Shamrock 500i Spectrograph (Andor, UK). A laser wavelength of 514.5 nm was used as the excitation source, with a 20 s exposure time and a 300 L mm^{-1} grating.

For the TEM analyses, the materials were deposited from ethanol on 200 mesh TEM copper grids covered with lacey carbon film. A Titan G2 80-200 TEM/STEM (FEI Company, The Netherlands) instrument with an image corrector was used to record the images at 200 kV accelerating voltage. Digital micrograph, ver. 2.12.1579.0 (for image recording), and TEM Imaging & Analysis, ver. 4.7 (for EDX analysis), were the software employed during the TEM investigation.

RESULTS AND DISCUSSION

Thermal decomposition in air

Thermoanalytical methods have been used to clarify the mechanism involved in the thermal decomposition of $[Ni(C_2O_4)(H_2O)_2]_n \cdot xnH_2O$, in both air and argon, as well as the decomposition products formed during its heating.

The TG, DTG and DTA curves, corresponding to the thermal decomposition in flowing air of $[Ni(C_2O_4)(H_2O)_2]_n \cdot xnH_2O$, are shown in Fig. 1a, while the FTIR curves of the gases evolved during the same process are shown in Fig. 1b.

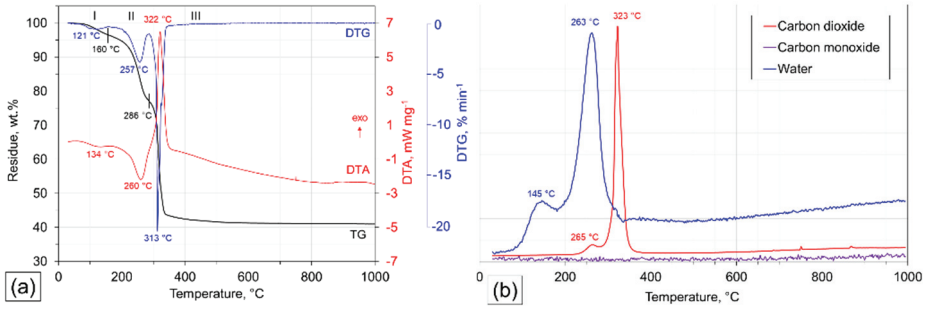

Fig. 1. Thermoanalytical curves for the thermolysis of $[Ni(C_2O_4)(H_2O)_2]_n{\cdot}xnH_2O$ in flowing air: a) TG, DTG and DTA results; b) FTIR analysis of generated gaseous products (not to scale): CO_2 2361 cm^{-1}, CO 2108 cm^{-1}, H_2O 1508 cm^{-1}.

The annealing was monitored by chemical analysis, XRD, FTIR, EDX and TEM.

Figs. 2 and 3 comparatively show the FTIR and Raman spectra of the coordination compound and its decomposition products.

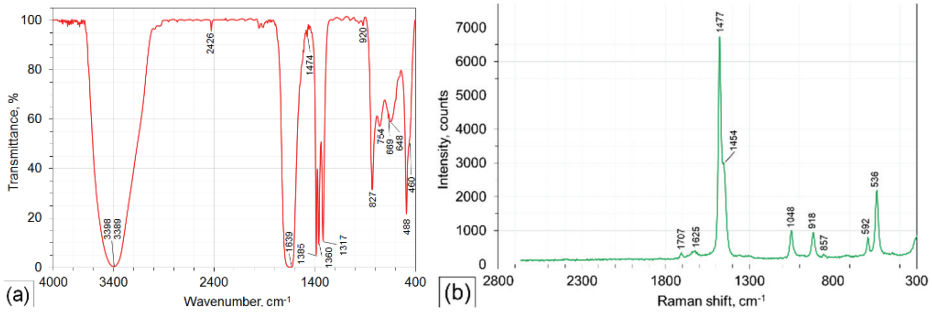

Fig. 2. FTIR (a) and Raman (b) spectra of the studied coordination compound.

The corresponding assignments of the FTIR and Raman spectra of $[Ni(C_2O_4)(H_2O)_2]_n{\cdot}xnH_2O$ are given in Table I.[11,20–25]

The intense FTIR band at 1639 cm^{-1} (Fig. 2a) is attributed to the asymmetrical vibration of the carboxylate ion. The value shows that the resonance from the carboxylate group is maintained during complex formation since the metal–carboxylate bond is preponderantly ionic. The band with the maximum at 1385 cm^{-1} is attributed to the ν_{sy}(OCO) symmetric vibration. The absence of the bands from the 1720–1660 cm^{-1} range, attributed to the ν_{asy}(C=O) vibration in the case of coordination compounds in which $C_2O_4^{2-}$ is coordinated as bidentate chelate ligand, shows that, in the synthesized complex compound, the resonance of the carboxylate groups is achieved, and that the four oxygen atoms are equivalent, the oxalate anion being a bridging ligand.[25] At the same time, the value for ν_{sy}(OCO),

i.e., 1385 cm^{-1}, along with the δ(OCO) found at 1317 cm^{-1}, are in agreement with the positions of the corresponding absorptions in oxalate-bridged complexes.[21] The very sharp and strong band at 488 cm^{-1} is attributed to the ν(Ni–O) vibration and/or ring deformation.

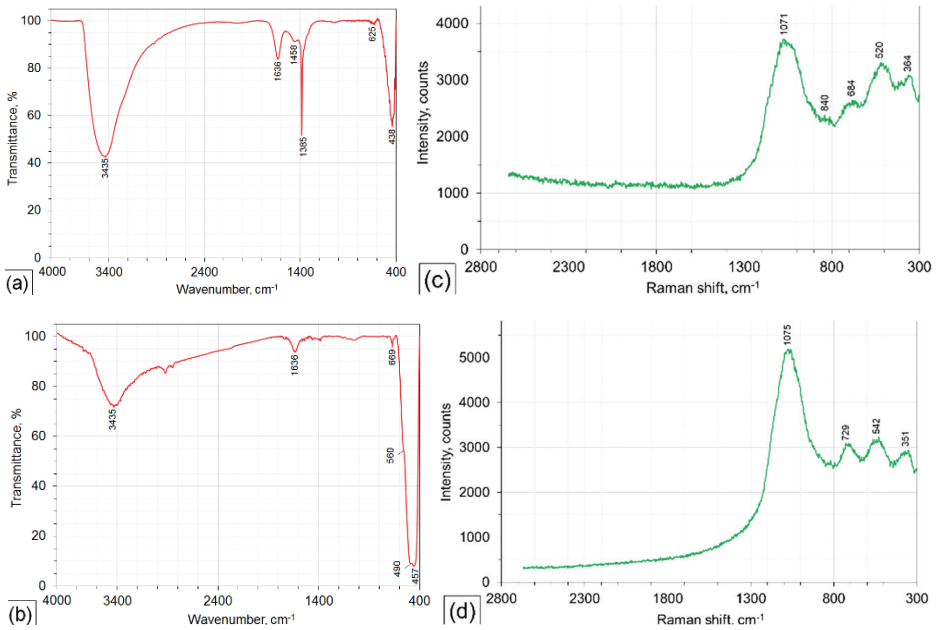

Fig. 3. FTIR (a, c) and Raman (b, d) spectra of the air decomposition products at 400 (a, c) and 1000 °C (b, d); the FTIR bands at 3435 and 1636 cm^{-1} are owned to traces of water.

TABLE I. Assignment of the FTIR and Raman spectra of $[Ni(C_2O_4)(H_2O)_2]_n \cdot xnH_2O$ (band positions are expressed in cm^{-1}); *vs* – very strong; *s* – strong; *m* – medium; *w* – weak; *br* – broad; *sh* – shoulder; H_2O* – coordinated water

FTIR	Raman	Assignments
3398/3389 *vs*, *br*		ν(OH) (H_2O), hydrogen bonding
	1707 *w*	ν_{asy}(C–O)
1639 *vs*, *br*	1625 *w*	ν_{sy}(OCO) + $\delta(H_2O^*)$
1474 *w*	1477 *vs*	ν_{sy}(C–O) + ν(C–C)
	1454 *s*, *sh*	ν_{sy}(C–O) + δ(OCO)
1385 *vs*		ν_{sy}(OCO)
1360 *vs*, 1317 *vs*		ν_{sy}(C–O) + δ(OCO)
	1048 *m*	ν_{sy}(C–O)
920 *w*	918 *m*	ν(C–C)
	857 *w*	ν(C–C)
827 *s*		ν_{sy}(C–C) + δ(OCO)
754 *m*, 669 *m*, 648 *m*		ρ(H_2O)
	592 *m*, 536 *s*	δ_{ring} and/or lattice water
488 *vs*, ~460 *sh*		ν(Ni–O) and/or δ_{ring}

The FTIR spectra of the thermal decomposition products show the characteristic bands of nickel oxide. In the case of the product obtained at 400° C (Fig. 3a), besides the two absorption bands of NiO at 625 and 438 cm^{-1}, other bands also appear and indicate the presence of traces of the partially decomposed coordination compound. At the same time, the FTIR spectrum of the product synthesized at 1000 °C (Fig. 3b) shows the absorption bands at 669, 560 (shoulder) and 457 cm^{-1}, slightly shifted with respect to the characteristic bands of nickel(II) oxide mentioned in the literature.[26] The more relevant bands of $[Ni(C_2O_4)(H_2O)_2]_n \cdot xnH_2O$, found at 1639, 1385, 1360, 1317, 827 and 488 cm^{-1}, are no longer present, leaving place for the two characteristic bands of nickel oxide. The other weak bands are not relevant for the decomposition of $[Ni(C_2O_4)(H_2O)_2]_n \cdot xnH_2O$. Also, the broadness of the 457 cm^{-1} band indicates that the NiO powder consisted of nanocrystals.[27]

After analysing the Raman spectra of the same products (Fig. 3c,d), the disappearance of the characteristic bands for the coordination compound can be observed, confirming its degradation. The more relevant bands, found at 1477, 1454, 1048, 918 and 536 cm^{-1} of $[Ni(C_2O_4)(H_2O)_2]_n \cdot xnH_2O$ (Fig. 2b), are replaced by the characteristic bands of nickel oxide. The Raman spectrum from Fig. 3d (for 1000 °C) shows the characteristic bands of nickel oxide (1075, 729, 542, 351 cm^{-1}) in accordance with literature data.[22,24] Also, the Raman spectrum from Fig. 3c (400 °C) reveals the presence of slightly shifted bands, confirming that it is, to some extent, contaminated with the traces of the partially decomposed precursor.

Based on the FTIR and Raman spectra, it can be concluded that nickel oxide as the final solid-state product is formed and $[Ni(C_2O_4)(H_2O)_2]_n \cdot xnH_2O$ entirely decomposed.

The XRD patterns of the powders obtained by the annealing of coordination compound at 400 and 1000 °C are presented in Fig. 4. Both patterns record the diffraction lines of the single-phase NiO (rhombohedral, ICDD file 01-078-4374). The powder annealed at 400 °C was composed of much smaller crystallites (4.4 nm) compared to the one annealed at 1000 °C (37.4 nm). For the powder annealed at 1000 °C, the calculated values of the lattice parameters, $a = b = 2.9575$ Å, $c = = 7.2464$ Å, are close to the values found in the ICDD file ($a = b = 2.9633$ Å, $c = = 7.2553$ Å).

These results allow some conclusions to be drawn based on the thermoanalytical curves presented in Fig. 1. The TG profile shows, in the first two steps, the removal of the lattice water and of the coordinated water molecules (mass loss: calculated 22.74 %; experimental: 22.89 %). Two endothermic DTA peaks located between 25 and 160 °C (weak maximum at 134 °C), as well as between 160 and 286 °C (maximum at 260 °C) and a change on the DTG curve in the same temperature ranges correspond to the removal of water. A completely dehydrated compound is produced at around 300 °C, as confirmed in Fig. 1b. These results are in

good agreement with literature data for nickel (II) oxalate dihydrate obtained through classical methods.[21,28] Also, the ratio between lattice water (3.57 % loss) and coordinated water (19.32 % loss), as calculated from the thermogravimetric analysis, shows for the $[Ni(C_2O_4)(H_2O)_2]_n \cdot xnH_2O$ formula that $x \approx 0.4$, which is slightly less than previously reported.[20]

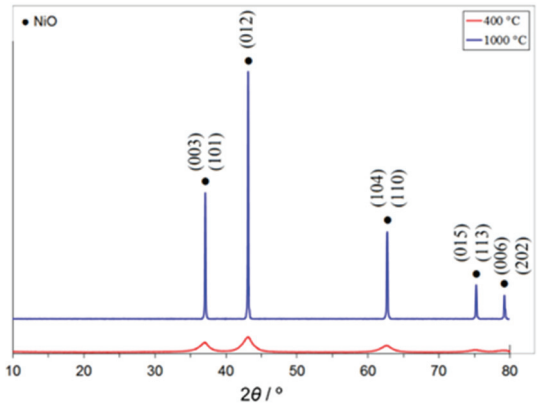

Fig. 4. XRD patterns of the powders obtained by the coordination compound's annealing at 400 and 1000 °C.

In the third step, the almost complete combustion of the anhydrous compound occurred within a narrow temperature range (286–345 °C), as shown by a steep slope on the TG curve with an inflexion point at 313 °C. The total experimental mass loss of 59.00 % (calculated 60.63 %) suggests NiO as the product of the conversion. The formation of this product was accompanied by a very sharp exothermic DTA peak located at 322 °C.

After analysing the FTIR curves from Fig. 1b, the water release can be confirmed due to the presence of two peaks: a weak one around 145 °C and the main one around 263 °C. The carbon dioxide shows a very intense peak at around 323 °C.

An EDX quantitative elemental analysis of very small areas revealed that, on the surface, the product obtained at 1000 °C in air is a non-stoichiometric oxide. The EDX profile for an area of the surface is presented in Fig. 5. It should be noted that the analysed area was smaller than 50 nm in diameter.

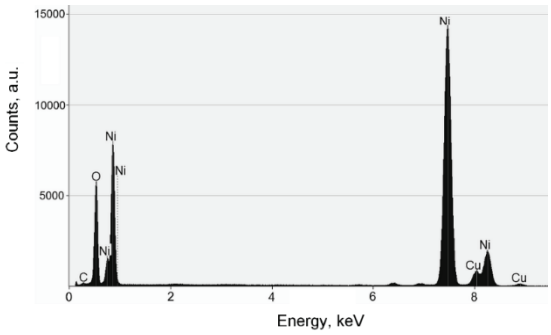

Fig. 5. EDX profile for a surface area (C and Cu peaks belong to the grid).

Table II shows the stoichiometry and composition of the nickel oxide analyzed by EDX.

TABLE II. Composition and stoichiometry of NiO obtained from EDX

Composition	wt. %	at. %
Ni	81.68	54.87
O	18.31	45.12
Ni:O (at. ratio)		1.2

The results indicate that, on the surface, the product is an oxygen-deficient non-stoichiometric nickel oxide.

The TEM analysis was performed to obtain useful information about the morphology and particle size of the nickel oxide originating from the thermal decomposition of the complex. TEM images recorded at different magnification values (Fig. 6) show that NiO was comprised of polygonal particles displaying some defined edges and faces, which appear to be further composed of small and conglomerated particles. The polygonal particles were piled up to form inter-particle pores of submicrometric sizes, corresponding to the spaces between them (Fig. 6a). The increase in magnification (Fig. 6b–d) did not allow for the improved particle differentiation. The formation of NiO aggregates, built from very small three-dimensional disordered primary particles, was clearly visible. The 2.07 nm value obtained from measurements performed on the TEM image shown in Fig. 6d corresponds to 10 interplanar spacings. The value for one interplanar spacing (2.07

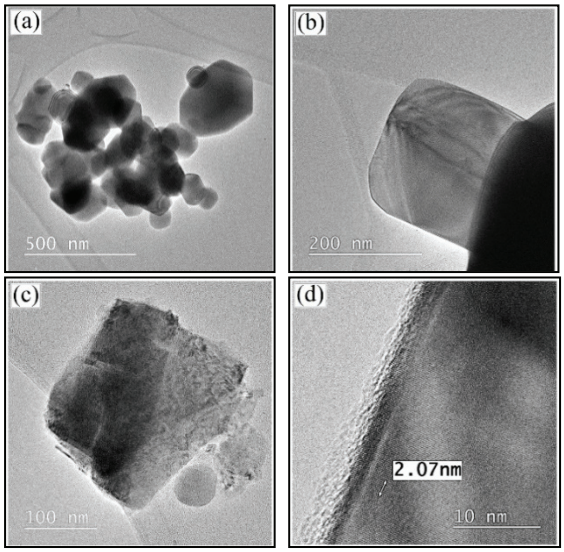

Fig. 6. TEM images of NiO obtained by decomposition of $[Ni(C_2O_4)(H_2O)_2]_n \cdot xnH_2O$ at 1000 °C in air atmosphere.

Å) is very close to the *d*-spacing of 2.095050 Å from the previously mentioned ICDD file 01-078-4374, which corresponds to the (012) crystal plane. Thermal decomposition of $[Ni(C_2O_4)(H_2O)_2]_n \cdot xnH_2O$ resulted in the formation of NiO with wide particle size distribution, from 4 nm to 1 μm.

Thermal decomposition in argon

The TG, DTG and DTA curves, corresponding to the thermal decomposition of $[Ni(C_2O_4)(H_2O)_2]_n \cdot xnH_2O$ in argon atmosphere, are shown in Fig. 7a, while the FTIR curves of the gases evolved during the same process are shown in Fig. 7b.

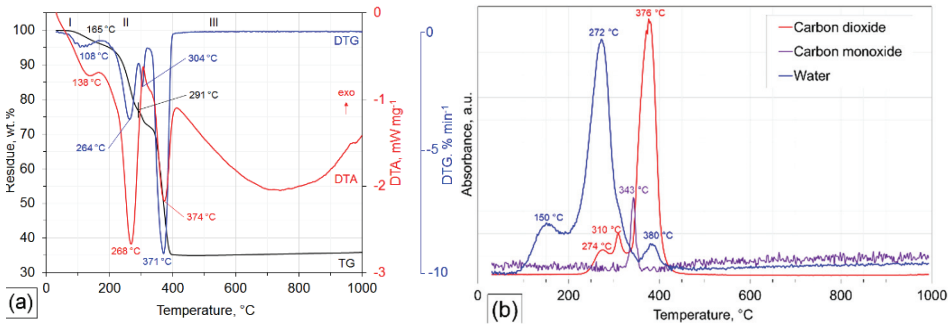

Fig. 7. Thermoanalytical curves for the thermolysis of $[Ni(C_2O_4)(H_2O)_2]_n \cdot xnH_2O$ in argon: a) TG, DTG and DTA results; b) FTIR analysis of generated gaseous products (not to scale): CO_2 2361 cm^{-1}, CO 2108 cm^{-1} and H_2O 1508 cm^{-1}.

As can be seen in Fig. 7, the TG profile shows, in the first two steps, the removal of the lattice water and of the coordinated water molecules (mass loss: calculated 22.74 %; experimental: 23.17 %). The first mass loss, up until around 165 °C, has a maximum intensity recorded at 108 °C and a corresponding endothermic DTA peak located at 138 °C, as confirmed by the FTIR spectrum (maximum at 150 °C). The second mass loss, up until around 291 °C, has a process maximum intensity at 264 °C and a corresponding endothermic DTA peak at 268 °C. This mass loss is also confirmed by the FTIR spectrum (maximum at 272 °C), which shows that the breakdown of the C–C bonds begins in this step and continues in step three (up until around 400 °C), with CO_2 release. A weak trace of CO was recorded in the third step at around 343 °C. The total mass loss of 65.01 % (calculated 65.66 %) suggests that the conversion product was a biphasic Ni/NiO system in a 3:2 molar ratio. The following analyses confirm this result.

The FTIR spectrum of the decomposition product in argon atmosphere is presented in Fig. 8. The spectrum shows a few absorption bands at 663, 555 (shoulder) and 476 cm^{-1}, slightly shifted compared with those from Fig. 3b, probably due to the presence of metallic nickel.

The XRD pattern of the powder obtained by annealing the coordination compound in argon at 1000 °C can be seen in Fig. 9. The XRD pattern records the

diffraction lines of the NiO (rhombohedral, ICDD 01-089-3080) and metallic nickel (cubic, ICDD 00-004-0850).

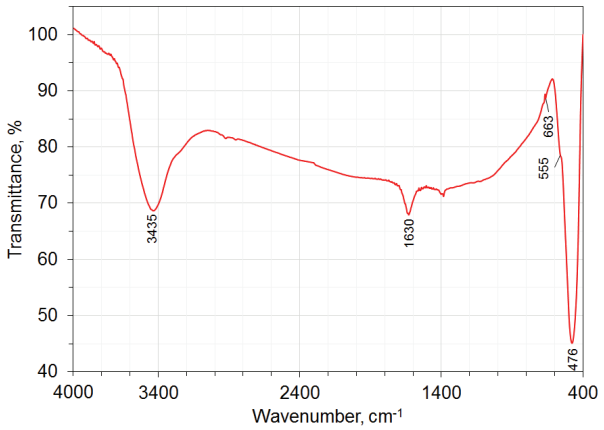

Fig. 8. FTIR spectrum of biphasic Ni/NiO system obtained by thermal decomposition at 1000 °C in argon atmosphere; the FTIR bands at 3435 and 1630 cm^{-1} are owned to traces of water.

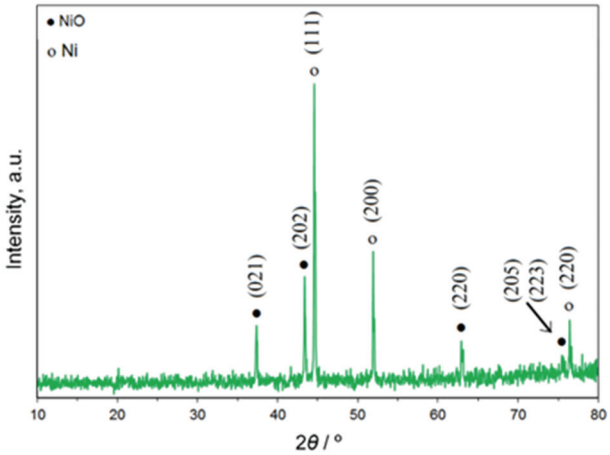

Fig. 9. XRD patterns of biphasic Ni/NiO system.

The TEM images of Ni/NiO at different magnification (Fig. 10) showed that the particles are of rhombohedral shape as well as the existence of submicrometric pores, which was already observed at NiO obtained in air atmosphere. The measurements performed on the TEM image presented in Fig. 10d show a value of 2.42 nm corresponding to 10 interplanar spacings. The value of 2.42 Å, corresponding to one interplanar spacing, is very close to the *d*-spacing of 2.412570 Å from the previously mentioned ICDD file 01-089-3080, which corresponds to the (021) crystal plane.

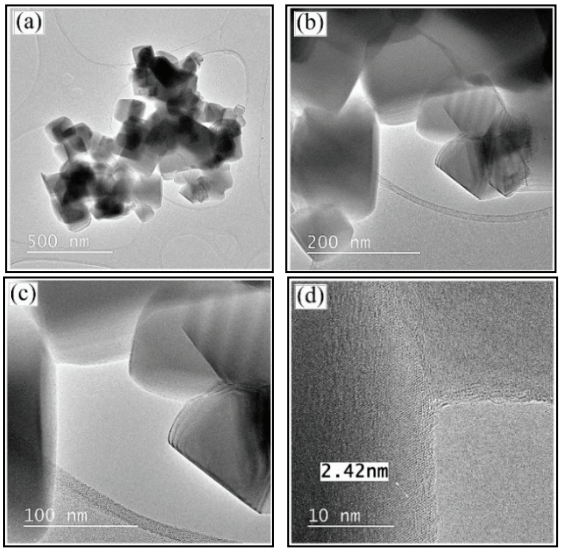

Fig. 10. TEM images of the NiO/Ni system obtained at 1000 °C in argon.

CONCLUSION

Three successive decomposition steps for $[Ni(C_2O_4)(H_2O)_2]_n \cdot xnH_2O$ were recorded during its thermal decomposition in dynamic air atmosphere, the first two being endothermic and the third exothermic.

The thermal conversion of this homopolynuclear coordination compound resulted in nickel oxide or a mixture of Ni and NiO in a 3:2 mole ratio, depending on the oxidative or inert atmosphere.

The XRD results reveal the rhombohedral crystallinity of the synthesized NiO phase and the cubic crystallinity of the metallic nickel phase. The TEM images at different magnification values show NiO particles obtained by the thermal decomposition of the coordination compound in air and consist of smaller particles. These particles exhibit polygonal shapes, and their size is widely distributed between 4 nm and 1 μm. The TEM images of the NiO/Ni system obtained in argon outline particles with rhombohedral shapes. For both oxidic systems, the particles were piled up and formed the inter-particle pores with sizes of tens of nanometers.

Acknowledgements. Part of this research was performed at the Center of Genomic Medicine of the "Victor Babes" University of Medicine and Pharmacy of Timișoara, POSCCE 185/48749, contract 677/09.04.2015. The authors wish to thank Prof. Dr. Zoltan Szabadai for some of the FTIR spectra and Dr. Maria Poienar for helping us obtain the ICDD files.

ИЗВОД

ТЕРМИЧКО ПОНАШАЊЕ ПОЛИМЕРНОГ КОМПЛЕКСА НИКЛ(II)-ОКСАЛАТА ДОБИЈЕНОГ РЕАКЦИЈОМ НИКЛ(II)-НИТРАТ/ЕТИЛЕН-ГЛИКОЛ

MIRCEA NICULESCU[1], MIHAI-COSMIN PASCARIU[2,3], ANDREI RACU[2] и BOGDAN-OVIDIU TARANU[2]

[1]University Politehnica Timisoara, Faculty of Industrial Chemistry and Environmental Engineering, 6 Vasile Parvan Blvd., RO-300223 Timisoara, Romania, [2] National Institute of Research and Development for Electrochemistry and Condensed Matter, 144 Dr. Aurel Paunescu-Podeanu, RO-300569 Timisoara, Romania и [3]"Vasile Goldis" Western University of Arad, Faculty of Pharmacy, 86 Liviu Rebreanu, RO-310414 Arad, Romania

Анализирано је термичко разлагање хомополинуклеарног координационог једињења $[Ni(C_2O_4)(H_2O)_2]_n \cdot xnH_2O$, полимерног комплекса никл(II)-оксалата. Термолиза је урађена у динамичкој оксидативној и инертној атмосфери истовременом применом термогравиметрије (TG), диференцијалне термогравиметрије (DTG) и диференцијалне термичке анализе (DTA). Предложени механизам разлагања је потврђен употребом технике анализе еволуираног гаса (EGA) путем инфрацрвене спектроскопије Фуријеове трансформације (FTIR) гасовитих производа разлагања. Производи у чврстом стању, који настају током загревања, испитивани су хемијском анализом, FTIR, Рамановом спектроскопијом и Рендгенском дифракцијом (XRD). Структура, морфологија и својства финалних производа разлагања су окарактерисани XRD, FTIR, енергетско дисперзивном рендгенском спектроскопијом (EDX) и трансмисијском електронском микроскопијом (TEM). Резултати анализа показују да је финални производ разлагања у оксидативној атмосфери никл-оксид, у облику полигоналних честица, док се у инертној атмосфери, добија смеша Ni и NiO у облику ромбоедарских честица у моларном односу 3:2.

(Примљено 13. октобра, ревидирано 25. децембра 2023, прихваћено 18. августа 2024)

REFERENCES

1. M. L. Grilli, *Metals* **10** (2020) 820 (https://dx.doi.org/10.3390/met10060820)
2. M. Niculescu, M. C. Pascariu, C. Muntean, V. Sasca, L. Lupa, M. S. Milea, M. Bîrzescu, *J. Therm. Anal. Calorim.* **131** (2018) 127 (https://dx.doi.org/10.1007/s10973-016-6079-1)
3. D. Roşu, M. Bîrzescu, M.-S. Milea, M.-C. Pascariu, V. Sasca, M. Niculescu, *Rev. Roum. Chim.* **59** (2014) 789 (https://revroum.lew.ro/wp-content/uploads/2014/9/Art%2009.pdf)
4. M. Niculescu, V. Sasca, C. Muntean, M.-S. Milea, D. Roşu, M.-C. Pascariu, E. Sisu, I. Ursoiu, V. Pode, P. Budrugeac, *Thermochim. Acta* **623** (2016) 36 (https://dx.doi.org/10.1016/j.tca.2015.11.008)
5. S. S. Narender, V. V. S. Varma, C. S. Srikar, J. Ruchitha, P. A. Varma, B. V. S. Praveen, *Chem. Eng. Technol.* **45** (2022) 397 (https://dx.doi.org/10.1002/ceat.202100442)
6. V. Biju, M. A. Khadar, *Mater. Sci. Eng., A* **304**–**306** (2001) 814 (https://dx.doi.org/10.1016/S0921-5093(00)01581-1)
7. F. Bødker, M. F. Hansen, C. B. Bender Koch, S. Mørup, *J. Magn. Magn. Mater.* **221** (2000) 32 (https://dx.doi.org/10.1016/S0304-8853(00)00392-9)
8. C. L. Carnes, K. J. Klabunde, *J. Mol. Catal., A* **194** (2003) 227 (https://dx.doi.org/10.1016/S1381-1169(02)00525-3)
9. G. Boschloo, A. Hagfeldt, *J. Phys. Chem., B* **105** (2001) 3039 (https://dx.doi.org/10.1021/jp003499s)
10. D. Das, M. Pal, E. Di Bartolomeo, E. Traversa, D. Chakravorty, *J. Appl. Phys.* **88** (2000) 6856 (https://dx.doi.org/10.1063/1.1312835)

11. Y. Wang, J. Zhu, X. Yang, L. Lu, X. Wang, *Thermochim. Acta* **437** (2005) 106 (https://dx.doi.org/10.1016/j.tca.2005.06.027)
12. X. Li, X. Zhang, Z. Li, Y. Qian, *Solid State Commun.* **137** (2006) 581 (https://dx.doi.org/10.1016/j.ssc.2006.01.031)
13. D. Y. Han, H. Y. Yang, C. B. Shen, X. Zhou, F. H. Wang, *Powder Tech.* **147** (2004) 113 (https://dx.doi.org/10.1016/j.powtec.2004.09.024)
14. X. Y. Deng, Z. Chen, *Mater. Lett.* **58** (2004) 276 (https://dx.doi.org/10.1016/S0167-577X(03)00469-5)
15. X. Xin, Z. Lü, B. Zhou, X. Huang, R. Zhu, X. Sha, Y. Zhang, W. Su, *J. Alloy Compd.* **427** (2007) 251 (https://dx.doi.org/10.1016/j.jallcom.2006.02.064)
16. A. Dierstein, H. Natter, F. Meyer, H.-O. Stephan, C. Kropf, R. Hempelmann, *Scr. Mater.* **44** (2001) 2209 (https://dx.doi.org/10.1016/S1359-6462(01)00906-X)
17. C. Lin, S. A. Al-Muhtaseb, J. A. Ritter, *J. Sol–Gel Sci. Tech.* **28** (2003) 133 (https://dx.doi.org/10.1023/A:1025653607374)
18. Y. R. Park, K. J. Kim, *J. Cryst. Growth* **258** (2003) 380 (https://dx.doi.org/10.1016/S0022-0248(03)01560-4)
19. Y. Wang, C. Ma, X. Sun, H. Li, *Inorg. Chem. Commun.* **5** (2002) 751 (https://dx.doi.org/10.1016/S1387-7003(02)00546-4)
20. M. Bîrzescu, M. Milea, D. Roşu, I. Ledeți, M. Rafailă, V. Sasca, M. Niculescu, *Rev. Roum. Chim.* **59** (2014) 555 (https://revroum.lew.ro/wp-content/uploads/2014/6/Art%2024.pdf)
21. E. D. Macklen, *J. Inorg. Nucl. Chem.* **30** (1968) 2689 (https://dx.doi.org/10.1016/0022-1902(68)80396-3)
22. N. Mironova-Ulmane, A. Kuzmin, I. Steins, J. Grabis, I. Sildos, M. Pärs, *J. Phys.: Conf. Ser.* **93** (2007) 012039 (https://dx.doi.org/10.1088/1742-6596/93/1/012039)
23. A. Wladimirsky, D. Palacios, M. C. D'Antonio, A. C. González-Baró, E. J. Baran, *J. Argent. Chem. Soc.* **98** (2011) 71 (https://notablesdelaciencia.conicet.gov.ar/bitstream/handle/11336/151619/CONICET_Digital_Nro.1f79f00b-4945-4466-aff5-917bfc14f1da_A.pdf)
24. M. Nowsath Rifaya, T. Theivasanthi, M. Alagar, *Nanosci. Nanotechnol. (Rosemead, CA, U.S.)* **2** (2012) 134 (https://dx.doi.org/10.5923/j.nn.20120205.01)
25. N. N. Dass, S. Sarmah, *J. Therm. Anal. Calorim.* **58** (1999) 137 (https://dx.doi.org/10.1023/A:1010148022032)
26. *Spectral Database for Organic Compounds, SDBS*, https://sdbs.db.aist.go.jp/sdbs/cgi-bin/direct_frame_top.cgi (accessed 25.09.2023)
27. H. Qiao, Z. Wei, H. Yang, L. Zhu, X. Yan, *J. Nanomater.* **2009** (2009) 795928 (https://dx.doi.org/10.1155/2009/795928)
28. X. M. Fu, Z. Z. Yang, *Adv. Mater. Res. (Durnten-Zurich, Switz.)* **228**–**229** (2011) 34 (https://dx.doi.org/10.4028/www.scientific.net/AMR.228-229.34).